Water Science & Technology

Water Science & Technology Vol 91 No 6, 731 doi: 10.2166/wst.2025.037

Differential overload simulation of condensate and housekeeping rendering wastewater for nutrient removal

Elias Daniel David Nova-Burgos[a,*], Diana Catalina Rodríguez-Loaiza[a] and Julio Cesar Saldarriaga-Molina[b]

[a] Pollution Diagnostics and Control Group (GDCON), Environmental School, School of Engineering, University Research Campus (SIU), University of Antioquia (UdeA), Cl 67 No. 53-108, Medellin, Colombia

[b] Grupo de Investigación en Infraestructura – GII, Environmental School, School of Engineering, University of Antioquia (UdeA), Cl 67 No. 53-108, Medellin, Colombia

*Corresponding author. E-mail: daniel.nova@udea.edu.co

EDDN-B, 0000-0001-5853-4230; DCR-L, 0000-0002-9310-6925; JCS-M, 0000-0002-9395-5417

ABSTRACT

The meat rendering process transforms waste from the meat industry to valuable materials as animal feed supplements. During the rendering process, large amounts of condensate and housekeeping wastewater (CWW and HKWW), solids and greenhouse gases are released into the environment imposing a huge pollution threat. Rendering condensate wastewater also causes many issues that commonly affect biological treatment processes such as pH inhibition, nutrient deficit and temperature. Therefore, the main objective of this work was to simulate the nutrient removal from a sequencing batch reactor (SBR) through the differential nitrogen overload of CWW. With aid of simulation, results found that the current SBR system does not remove carbon and nitrogen as much as other biological systems. This is due to low biodegradation of chemical oxygen demand (COD), the high content of inert particulate carbon (XI), identified in the fractionation of HKWW, and the toxic and inhibitory effect of ammonium present in CWW. When the system is overloaded with nitrogen from CWW there is little removal of biochemical oxygen demand (BOD), ordinary heterotrophic organisms (OHO) outnumber autotrophic nitrifying organisms (ANO) and ammonium toxicity occurs, all contributing to a failure to remove nutrients.

Key words: biodegradability, condensate wastewater, housekeeping wastewater, nutrient removal, pH inhibition, simulation

HIGHLIGHTS

- The biological treatment process remains a key area of study due to its sustainability.
- Wastewater simulation offers a cost-effective way to manage complex treatment systems.
- The lack of data from measurement campaigns is a common constraint in simulation exercises.
- Counting biokinetic parameters is key to reducing time spent in calibration.

1. INTRODUCTION

Meat rendering is one of the oldest examples of a circular economy, transforming waste materials (byproducts, up to 33% of each produced animal) from meat industry activities into useful products such as animal feed additives (protein meals for livestock), soaps and rustproofing paints (Kosseva 2020). The meat rendering process generates two main streams: the condensate and housekeeping wastewaters (CWW and HKWW). Both produce large amounts of hydrolyzed fat, oil, grease (FOG), and proteins that trigger socio-environmental impacts (Pintor *et al.* 2016; Sanghamitra *et al.* 2021).

Biological processing, one of the most practical, sustainable, and economically achievable technologies, is commonly affected by meat rendering wastewater since hydrolyzed FOG reduces the transport rate between cells and the aqueous phase (Sultana *et al.* 2024), exposes microorganisms to inhibition (e.g. nitrifiers) and washout due to the toxic effect of long chain fatty acids (LCFA) and volatile fatty acids (VFAs) (Klaucans & Sams 2018; Brennan *et al.* 2021). Moreover, this type of effluent leads to micronutrient deficiencies, such as a low nitrogen and phosphorus ratio, because the materials arrive in an advanced state of decay. This results in longer wastewater storage times and, consequently, a more pronounced phosphorus nutrient deficit. This nutritional deficit impacts essential bio-communities for the secondary treatment as ordinary heterotrophic organisms (OHO), autotrophic nitrifying (ANO) compounds by the growth of ammonia-oxidizing bacteria (AOB), nitrite-oxidizing bacteria (NOB), and polyphosphate-accumulating organisms (Sanghamitra *et al.* 2021). Finally, the secondary process is also affected by the high heat transfer (temperature up to 40 °C) from condensate wastewater which promotes filamentous and viscous sludge bulking, damaging the solid settling, and hereafter the removal of effluent total suspended solids (TSS) (Bedoić *et al.* 2020).

To account for the complexity of biological processing, plant-wide models (simulations based on mathematical understanding) became a great alternative to meet standards. Thus, plant-wide models are now suggested as an alternative to control interfaces and components, retrofitting, optimize operational plant cost, aid in the operator's training, control evaluation ('what if?' scenarios), optimize removal efficiency, energy recovery (e.g. biogas) (Chen *et al.* 2020) and to keep an eye on energy balances (Muster-Slawitsch *et al.* 2021), process risk, and life cycle assessment (Makinia & Zaborowska 2020).

Although many biological process representations exist, such as statistical, numerical optimization, and artificial neuronal nets, few studies have examined meat-rendering wastewater using biokinetic models controlled by rational and mathematical approaches. Nowak *et al.* (1996) investigated the kinetics of nitrification in continuous activated sludge (AS) under phosphorus deficiency. Nakhla *et al.* (2006) modeled the reaction kinetics of an aerobic batch-AS system and suggested correction of modeling for biomass growth and hydrolysis by Monod's models. Finally, regarding SBR systems, Conde & Kaparaju (2022) examined the temporal variation in the chemical composition of methane production of rendering wastewater (RWW) with a hydrolysis model representation of Gompertz.

One of the biggest challenges for many practitioners is the lack of data from measurement campaigns and biokinetic parameters due to high cost. Thus, an alternative is to use influence and model parameters as a reference to improve the calibration. However, there are no current reference parameters for the combined effect of the nitrogen overload with CWW into the HKWW. Despite this limitation, this document provides complete data and thorough reports on simulations to highlight relevant details and understanding of the effect of CWW.

While previous research has explored aspects of nutrient removal and methane production, the novelty of this research lies in giving insights into the most important influent fractionation and biokinetic model parameters. This study provides (a) a reference that can reduce time spent on future simulations, (b) an analysis of the impact of the overload of nitrogen of CWW into the HKWW ratios, (c) an evaluation of the plant performance at the lower cost which has not been simulated before, as a sustainable alternative to wastewater treatment instead of chemical use.

2. METHODS

The methodology followed the recommendations of the unified simulation protocol from the IWA task group on good modeling practices that were evaluated in more than 100 domestic wastewater plants and upgraded industrial effluents, such as a soy sauce plant (rich in nitrogen) that was composed of bean processing, brewing, and bottling (Rieger *et al.* 2012).

2.1. Project definition

Data for this study were taken from Agropecuaria San Fernando S.A (AGROSAN), a rendering protein recovery plant located 36 km from Medellin in the town of Amaga, Antioquia, Colombia (06°03′N, 75°41′O). At 1,496 m MSL and a mean temperature of 21 °C, the plant produces meal and fat products for the animal feed from meat byproducts (viscera, feathers, blood, tallow, bone, and fat), which originate from slaughterhouses of cattle and pigs , chicken slaughter farms, and the meat industry sector. The complete meat-rendering plant (Figure 1) produces two major wastewater streams known as 'condensate 2.1' (2.5 L/s) of the meal production and 'housekeeping (1)' of the overall plant cleaning (1.7 L/s) that were treated in the SBR highlighted in red in Figure 1.

2.2. Data collection

The original state variables for this project were gathered, collected, preserved, and transported to the research group Grupo Diagnostico y Control de la Contaminación from the Universidad de Antioquia by Rodríguez *et al.* (2011) for a series of 50 daily data samples taken over 8.4 months at the meat by-product plant. Influent and effluent data were composed and measured by the next series of analytical parameters: chemical oxygen demand (COD), biochemical oxygen demand on the fifth day (BOD_5), ammonia (NH_4^+), nitrite (NO_2^-), nitrate (NO_3^-), polyphosphates (PO_4^{-3}), sulfates (SO_4^-), potential of hydrogen (pH), temperature, conductivity, and sludge composition by total solids (TS), volatile solids (VS), total suspended

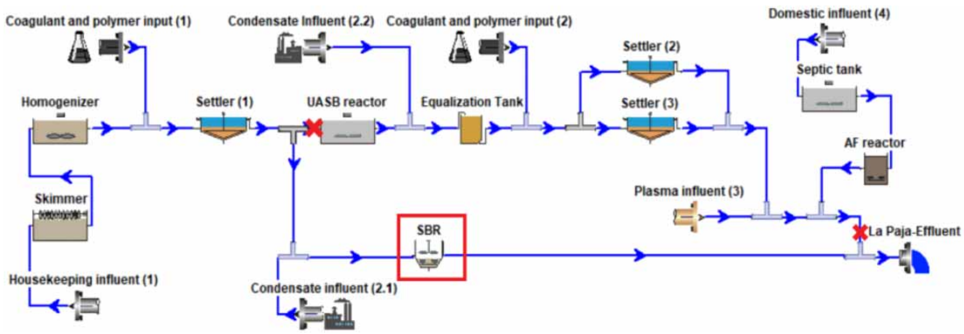

Figure 1 | Liquid line production scheme of the whole rendering plant and SBR location of study (red square), the SBR system treats the pretreated housekeeping (1) and condensate influent (2.1 and 2.2). *Source*: Own elaboration using BioWin-6.2 software®.

solids (TSS), volatile suspended solids (VSS), and sludge volume index (SVI). For more information, readers are encouraged to refer to the study of Rodríguez *et al.* (2011).

2.2.1. SBR physic parameters

The characteristics of the SBR reactor used by Rodríguez *et al.* (2011) are described below. The fiberglass SBR system is comprised of a 2.92 m^3 volume capacity (1.466 m^3 for reacting and 0.733 m^3 as minimum level), a programmable logic controller that turns on or off the equipment parts as the submerged aerator, a pump, and a stirring system. The maximum hydraulic load capacity equals three cycles of 0.733 m^3 (minimum level) in 1 day or 2.19 m^3/day (0.025 L/s). The cyclic operation process includes filling, reaction, sedimentation, and drawing and idling of the system. This process takes place three times a day in 8-h cycles. The filling stage lasts 35 min, in which every 2 h of the reaction phase one-third of the filling pulse is pumped into the system (0.244 m^3). Next, there are 6 h of the reaction phase consisting of 8 min of intermittent aeration and 15 min of stirring without aeration. The underflow is carried out 15 min before the aeration ends. Finally, for the remaining 2 h, the sedimentation is carried out, with the last 5 min being the decanting phase.

2.3. Plant model setup

The plant model layout for the optimization is composed of influent, SBR, effluent, and underflow wastage-WAS (Figure 2). The general parameters for the SBR system and pre-running simulation with default parameters are set to check the hydraulic (transport model) and prepare the software before any formal simulation.

2.3.1. Bioreactor model

The conversion model (microbiological scale) was defined as the general biokinetic AS/anaerobic digestion model ($ASDM_i$) which has more than 50 state variables, 80 process expressions (Envirosim 2021), 24 processes for growth, and decay of ordinary heterotrophic organisms (11 kinetic parameters, 30 stoichiometric parameters, 4 pH inhibition parameters, and 9 switching functions), 10 processes for hydrolysis, adsorption, ammonification, and assimilative denitrification (9 kinetic parameters, 4 stoichiometric parameters), 4 processes for the growth and decay of ammonia-oxidizing biomass (9 kinetic parameters, 7 stoichiometric parameters, 2 pH inhibition parameters, and 4 switching functions), and 2 processes for the growth and decay of nitrite-oxidizing biomass (5 kinetic parameters, 10 stoichiometric parameters, 2 pH inhibition parameters, and 5 switching functions). Lopez-Vazquez *et al.* (2017) and Van Loosdrecht *et al.* (2015) broadly recommend the use of biokinetic models for nitrogen removal simulation.

2.3.2. Pseudo steady-state

Due to the dynamic nature (timescale) of the SBR system, a pseudo-steady state should be reached before the simulation analysis to avoid bias in effluent results. This state is achieved around 2 SRT to equalize short-term variations (Orhon *et al.* 2009) or by viewing the establishment of the TSS response in the TSS vs time graph (Casellas *et al.* 2008).

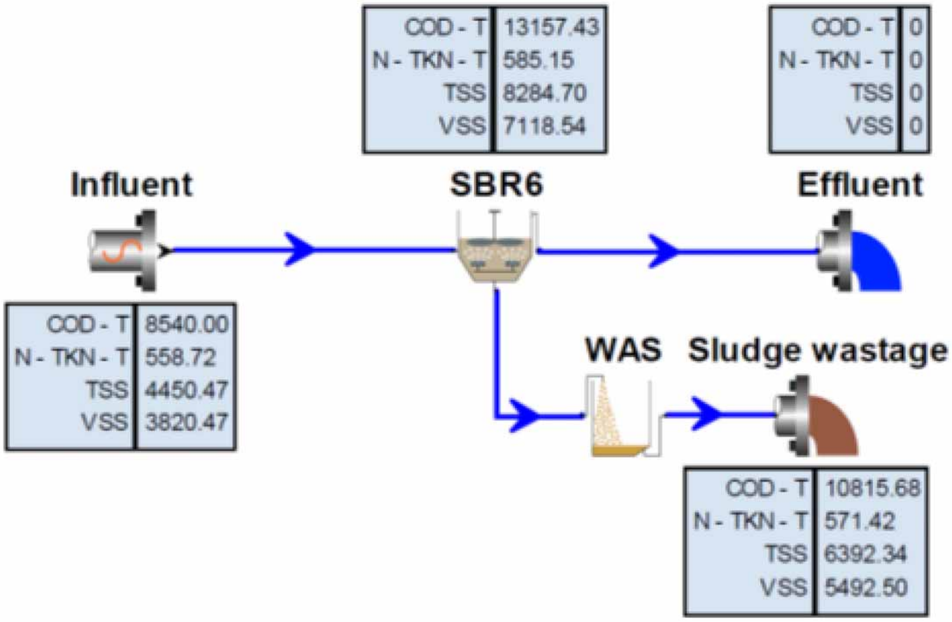

Figure 2 | SBR flowsheet for the meat byproducts plant. *Source*: BioWin-6.2 software®.

2.3.3. Operational SBR conditions

The operational conditions are configured by the SBR dimensions, itinerary setting, aeration schedule, temperature rating, SRT, influent rates, and sink streams. In relation to SBR dimensions, the minimum decant level (liquid hold-up) was selected as 50% of the reaction tank. The itinerary (cycle) setting was set up as follows: 8 h of the cycle length of duration, mix until settling at 6 h, and draw effluent starting at 7:55 h (i.e. 5 min at the end of the cycle). The aeration method is a dissolved oxygen (DO) setpoint approach (instead of airflow input), which is set as an intermittent itinerary aeration option, i.e. 1.1 mg O_2/L for 8 min aeration and 15 min aeration, turned on and off repeatedly, until 360 min (6 h). The operative average temperature value was fixed as 21 °C in the Project/Plant/Liquid temperature option. While the SRT project was set as 30 days as the quotient between the mass of sludge in the reactor over the mass of sludge dumped per day, to promote the growth of nitrifying bacteria (Rodríguez *et al.* 2011), this parameter never should fall behind 5–10 days for biological nutrient removal plants to work properly, when ensuring enough oxygen supply. Three loads from influent flow rates of 0.24333 m^3 (1/3 of 0.73 m^3) are delivered to the SBR tank at 0, 2, and 4 h, which means that every 2 h an incoming flow of 10.01 m^3/day is pumped during 35 min, similar to reports by Oles & Wilderer (1991) and Corominas Tabares (2006). Moreover, the hydraulic retention time (HRT) is equal to 16 h, where the total volume is 1.46 m^3, and the inflow is 3 times 0.73 m^3/day.

There are two types of sink streams: the decant and the underflow rates. The decant flow rate (210.24 m^3/day) is set by default calculation by the BioWin simulator software according to the drawn timespan (5 min) and the minimum decant level (50%). The underflow rate was equal to 0.0487 m^3/day and the reactor will be wasted as underflow from the mixed liquor volume during the last 15-min phase of mixing (from 5.75 to 6 h).

2.4. Calibration

Calibration is adjustments and estimations to enhance the good of fitness between simulated and observed values (Makinia & Zaborowska 2020). The process engineering calibration was performed and a static sensitivity analysis was adapted for influent fractions and model parameter calibration in the next stepwise procedure and modified from Rieger *et al.* (2012): The first calibration stage included sludge production variables such as TSS, VSS, and inert suspended solids (ISS) from the mixed liquor (MLVSS), the effluent, and the wastage underflow, where the most sensible variables were the maximum growth and decay of OHO, and the hydrolysis constant rate. The next calibration stage was the influent organic VFAs fractions (S_A) as acetic acid for targeting the BOD_5 and COD concentrations at the effluent. In the last calibration stage, nitrogen response concentrations NH_4^+ were calibrated for nitrification by changing the maximum growth and decay of AOB (μ_{Ammonia}, b_{Ammonia}), and NO_2^-, NO_3^- for denitrification at the effluent.

2.4.1. Calibration evaluation

The mean absolute percentage error (MAPE) is used to measure the best fit and compare the degree of prediction between models with varying scales (Hauduc *et al.* 2015). The MAPE (Equation (1)) is calculated using the software R-4.0.2.®, packages 'MLmetrics' and function 'mape_value' and its optimal value is zero (Moreno *et al.* 2013).

$$\text{MAPE} = \frac{1}{n} * \sum_{i=1}^{n} \left(\frac{|y_{i,\,\text{obs}} - y_i|}{|y_{i,\,\text{obs}}|} \right)^2 \quad (1)$$

where n is the total number of experimental data points for the output variable y. $y_{i,\text{obs}}$ is the observed (measured) data at point I, and y_i is the model prediction value at point I.

Since MAPE quantifies the average magnitude of model errors, the MAPE of TSS, COD, and BOD of 44, 22, and 34%, respectively (Figure 3), can be considered reasonable predictions (20–50%), and could benefit from further calibration. While MAPE of NH_4^+ of 1.23% is very accurate (<10%), which indicates that it is acceptable for nutrient removal analysis. Other authors like Rieger *et al.* (2012) from the good modeling practice group from the International Water Association (IWA), suggest a TSS error of 10% for nitrogen removal, but in practical experience, Makinia & Zaborowska (2020) recommended that the typical range of error should vary from 5–20% to 10–40% for steady-state and dynamic predictions, respectively.

2.5. Simulation of the differential nitrogen overloading with CWW

To determine the maximum ratio of CWW that could be mixed with the HKWW to yield the best nutrient removal and comply with the local discharge limits, the SBR system operates by changing the percentage of housekeeping and condensate wastewater ratios in a lumped matrix under eight different nitrogen overload stages with CWW (Table 1). For reference, the SBR system has a maximum hydraulic capacity of 0.73 m^3/day, which does not change over time. The inlet ratio for stages I, II, and III is a compound of 100% HKWW, and then stage IV is a compound of 90% HKWW and 10% nutrient overload of CWW, similar to the rest of the stages. Stage VIII contains 0% HKWW and 100% CWW overload.

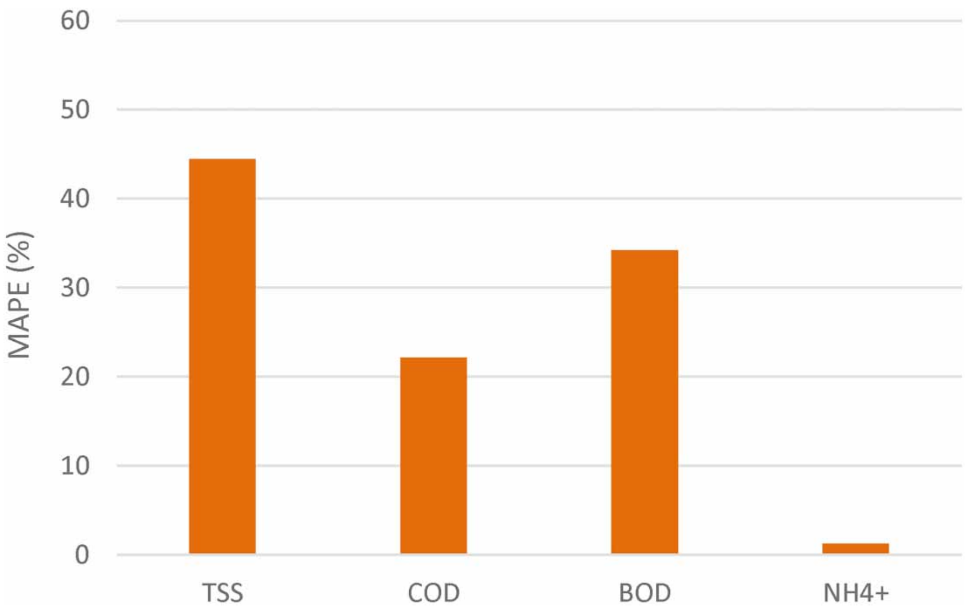

Figure 3 | Calibration assessment with fractionation average and model parameter modification.

Table 1 | Operational nitrogen overloading stage with CWW in the SBR system

Stages	Time of operation (days)	Mix ratio	
		Housekeeping wastewater (%)	Condensate wastewater (%)
I	0–21	100	0
II	22–43	100	0
III	44–77	100	0
IV	78–98	90	10
V	99–154	80	20
VI	155–189	50	50
VII	190–231	30	70
VIII	232–252	0	100

Source: Own elaboration based on Rodríguez *et al.* (2011).

2.5.1. Influent data completion

The total influent compositions of both HKWW (stages I, II, and III) and CWW (stage VIII) are already known. However, missing data from stages IV to VII are unknown, thus, the missing data are pondered according to the percentage of differential overload (weighted average fashion). For instance, the calcium content of any data belonging to stage V is computed as the calcium concentration for HKWW times 0.8 (80% of overload) plus the calcium concentration of CWW times 0.2 (20% of overload) and everything divided by 1 (or 100%).

2.5.2. Influent data fractionation

Influent fractionation was carried out following the fractionation methodology of the Dutch Foundation of Applied Water Research (STOWA) protocol, available in Makinia & Zaborowska (2020) table 6.9. COD materials are integrated in soluble non-biodegradable (inert) COD (S_I), particulate non-biodegradable (inert) COD (X_I), readily biodegradable COD (S_S), and slowly biodegradable COD (X_S). Influent characterization of nitrogenous materials is represented in terms of total Kjeldahl nitrogen (TKN), NO_3^-, and NO_2^-. TKN is divided into free and saline ammonia (S_{NH}) and organically bound TKN. The organically bound TKN is divided further into two portions: biodegradable and non-biodegradable each with soluble and particulate sub-portions. The particulate non-biodegradable portion is associated with the particulate non-biodegradable COD, and, therefore, leaves the system via the sludge wastage (Melcer 2004).

Similar to missing data completion, the fractionation of the differential overload data was weighed between housekeeping and condensate wastewater according to the overload ratio. For instance, the inert soluble COD fraction of stage VI is computed as the S_I fraction of stage II (HKWW) times the overload percentage 0.5 (50%) plus the S_I fraction of stage VIII (CWW) times the overload percentage 0.5 (50%) and everything divided by 1 (or 100%). Table 2 summarizes the fractionation results of the differential overload project.

2.5.3. Model parameter configuration

The most relevant model parameter modifications, such as maximum growth of OHO and carbon hydrolysis, are 70–90% lower than observed in domestic wastewater, as found in Nakhla *et al.* (2006) and Conde & Kaparaju (2022). Model parameters are also weighted in proportion to the differential overload for influent data completion. The hydrolysis rate constant (K_H) of stage VII is computed as K_H of stage II (HKWW) times the overload percentage 0.3 (30%) plus the K_H fraction of stage VIII (CWW) times the overload percentage 0.7 (70%) and everything is divided by 1 (or 100%). Table 3 summarizes the modification of model parameters of the differential overload project.

2.6. Validation

The J^2 coefficient (Equation (2)) will be adopted for the validation (model checking) to evaluate the change in model efficiency between calibration and validation steps. Validation is calculated using the software R-4.0.2.®, packages 'hydroGOF', and function 'gof'. In general, one additional measurement point of each simulation stage was preserved for

Table 2 | Biowin fractionation input for the differential load of wastewater

Fraction/composition	Pseudo-steady state 100%/0%	Stable response housekeeping (%)/condensate wastewater (%) Stage I 100%/0%	Stage II 100%/0%	Stage III 100%/0%	Stage IV 90%/10%	Stage V 80%/20%	Stage VI 50%/50%	Stage VII 30%/70%	Stage VIII 0/100%
1 (S_S)	0.7874	0.3282	0.3282	0.3282	0.3739	0.4197	0.5569	0.6484	0.7857
2 (S_A)	0.1785	0.4445	0.4445	0.4445	0.4181	0.3917	0.3124	0.2595	0.1802
3 (X_{sp})	0.9500	0.9500	0.9500	0.9500	0.9500	0.9500	0.9500	0.9500	0.9500
4 (S_I)	0.0176	0.0219	0.0219	0.0219	0.0241	0.0262	0.0327	0.0370	0.0434
5 (X_I)	0.1090	0.5206	0.5206	0.5206	0.4757	0.4307	0.2959	0.2061	0.0713
6 (F_{cel})	0.9500	0.9500	0.9500	0.9500	0.9500	0.9500	0.9500	0.9500	0.9500
7 (S_{NH4})	0.9605	0.9046	0.9046	0.9046	0.9094	0.9142	0.9286	0.9383	0.9527
8 (X_S*iN_{XS})	0.0007	0.0163	0.0163	0.0163	0.0147	0.0132	0.0085	0.0055	0.0008
9 (S_I*iN_{SI})	0.0001	0.0021	0.0021	0.0021	0.0020	0.0018	0.0014	0.0011	0.0006
10 (N/COD)	0.0700	0.0911	0.0911	0.0911	0.1389	0.1867	0.3301	0.4257	0.5691
11 (SPO_4)	0.4098	0.2323	0.2323	0.2323	0.2500	0.2678	0.3211	0.3566	0.4098

Note. Fractions are ordered according to the BioWin input prompt.
Source: Own elaboration applying the STOWA fractionation protocol.

Table 3 | Biowin fractionation input for the differential load of the housekeeping and rendering wastewater

Model parameter	Pseudo-steady state 100%/0%	Stable response housekeeping (%)/condensate wastewater (%) Stage I 100%/0%	Stage II 100%/0%	Stage III 100%/0%	Stage IV 90%/10%	Stage V 80%/20%	Stage VI 50%/50%	Stage VII 30%/70%	Stage VIII 0/100%
$\mu_{H,max}$	0.5000	0.5000	0.5000	0.5000	0.5730	0.6460	0.8650	1.0110	1.2300
b_H	0.1000	0.1000	0.1000	0.1000	0.0950	0.0900	0.0750	0.0650	0.0500
K_H	0.5000	0.5000	0.5000	0.5000	0.4940	0.4880	0.4700	0.4580	0.4400
$\mu_{Aut,max}$	0.3600	0.3600	0.3600	0.3600	0.3740	0.3880	0.4300	0.4580	0.5000
b_{Aut}	0.2000	0.2000	0.2000	0.2000	0.1900	0.1800	0.1500	0.1300	0.1000

Note. Parameters presented the highest sensitivity on the calibration.

the validation (i.e. 8 from 8 differential nitrogen overloading stages).

$$J^2 = \left(\frac{\frac{1}{n\_val} * \sum_{i=1}^{n\_val} (y_{i,\,obs} - y_i)^2}{\frac{1}{n\_cal} * \sum_{i=1}^{n\_cal} (y_{i,\,obs} - y_i)^2} \right) \quad (2)$$

where n is the total number of experimental data points for the output variable y; $y_{i,obs}$ is the observed (measured) data at point I; y_i is the model prediction at point I; and n_cal and n_val are the total number of measurements used in the calibration and validation periods, respectively.

J^2 coefficient was close to 1 (Figure 4), indicating that it was relatively acceptable for four variables (Makinia & Zaborowska 2020). When the J^2 is much higher than 1, it could indicate either a change in model structure or a lack of robustness due to model over-fitting. The lower change in efficiency was for the BOD_5 variable (0.6333 J^2 in Figure 4) due to the further improvement needed in the S_A fraction, analyzing acetic acid as an S_A reference. Brennan *et al.* (2021) and Conde & Kaparaju (2022) found that additional VFAs fractions (S_A), such as propionic, butyric, and valeric also determine the organic concentrations and the influence in the pH inhibition.

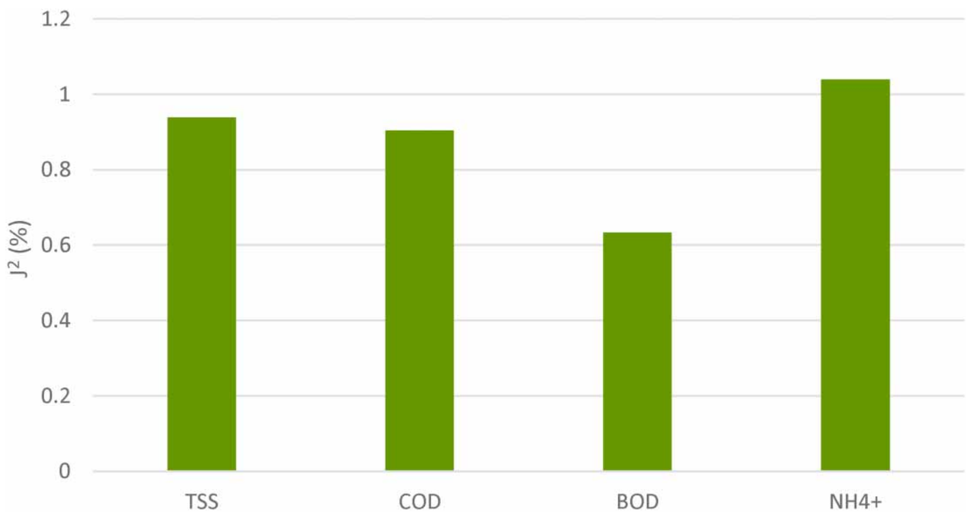

Figure 4 | Validation assessment with fractionation average and model parameter modification.

3. RESULTS

3.1. Solid phase

3.1.1. Total suspended solids

The pseudo-steady state was simulated 60 days (2 SRT) before day 0 of measurement data and the microorganism's establishment occurred on day 12 of simulation, as presented in the mass balance chart (Figure 5). This graphic also presents a solid overload from stage V (80% of HKWW and 20% of CWW), especially from the HKWW as a consequence of grease and oil overload, which contains a high particulate inert carbon content (X_I, on stages I–III from Table 2). Poor settleability (SVI = 450 mm/h) is seen as well and impacts the TSS, COD, and BOD removal due to its low biodegradability, as also found by Conde & Kaparaju (2022). Microorganism wash-out refers to the biomass loss from the reactor, commonly due to an increment of the incoming flow, as regularly occurs in most of the treatment plants (e.g. by wet peak discharge). In this case, however, the solid and nutrient overload does not physically wash microorganisms out of the system since the influent hydraulic load is constant. What causes biomass wash-out (loss) is the harsh environmental conditions that inhibit biomass growth and increase decay. The acute inhibition due to the failure in the coagulation process prior to the SBR (Figure 1), is caused by the high grease and oil input. Nakhla *et al.* (2003) also treated and simulated rendering wastewater and stated that the high oil and grease caused a 57–70% degradation rate reduction in apparent biomass due to strong inhibition and nutrient deficit.

3.1.2. Sludge retention time-SRT

As shown in Figure 6, the trend shows that under regular inflow load, the SRT remains at 30 days, but when the possible nutrient overload of grease and oil (inert COD) occurred, the SRT was reduced (washed-out) by half of its original value, as also

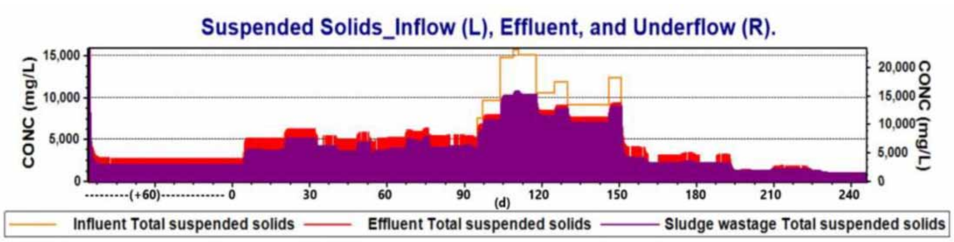

Figure 5 | Solids/mass balance chart: influent TSS concentration at the left axis (L), while the effluent and underflow stay at the right axis (R). *Source*: Own elaboration running the BioWin software®.

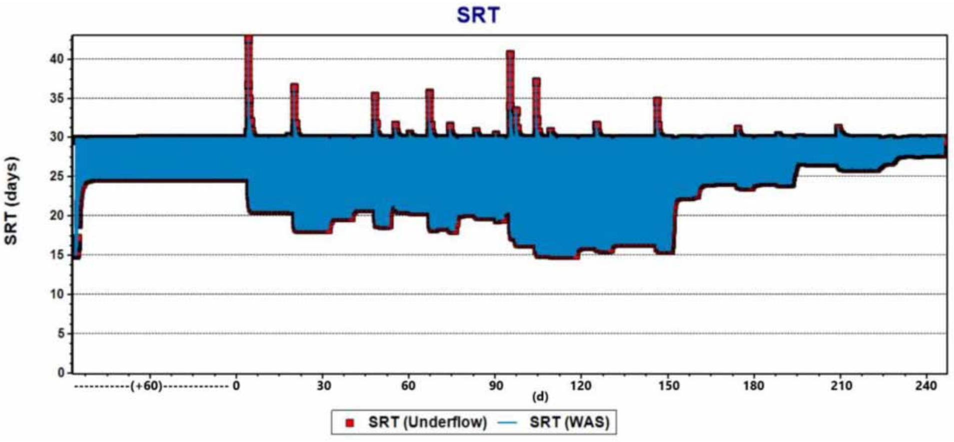

Figure 6 | SRT chart: sludge retention time under differential overloading of CWW.

found by Conde & Kaparaju (2022). This enormous issue is largely due to not having enough ready carbon entering the system to promote cellular growth and not allowing the right mass transport into the microbial cells due to the hydrophobic nature of lipids (Brønd & Sund 1994) as could happen in stage V.

3.2. Liquid phase

3.2.1. Influent concentration

As shown in Figure 5, the system also presents an unusual carbon overload during stages IV and V (upper blue line, Figure 7). This is a result of the high soluble inert carbon fraction (S_I) from the grease and oil overload, which triggers very difficult environmental conditions for the normal growth of heterotrophic and nitrifying bacteria. This figure also shows that the HKWW contains high carbon (around 8,308 mg COD/L) and low nitrogen concentration (365 mg NH_4^+-N/L, lower pink line in Figure 7) until day 77 (i.e. stages I, II, and III). In contrast, the CWW contains high nitrogen concentration (615 mg NH_4^+-N/L) and lower carbon load (1,381 mg COD/L), from day 233 to 252 (i.e. stage VIII). Additionally, the COD/N or COD/P ratios are lower for the CWW than for HKWW, but the CWW is more 'biodegradable' than the HKWW, as presented in Table 2. The former contains a higher readily biodegradable COD fraction (S_S), while the latter contains higher soluble and particulate inert COD fractions (S_I and X_I).

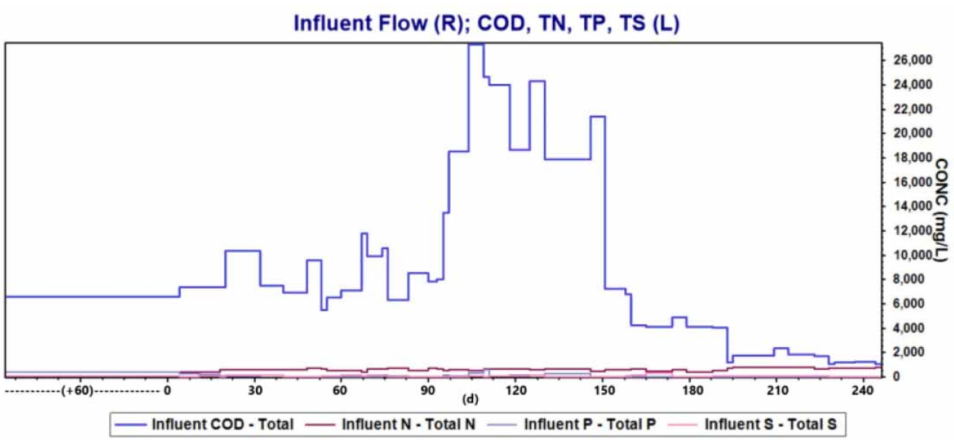

Figure 7 | Flow/nutrient chart: influent flow and nutrient concentration of nitrogen, phosphorus, and sulfur.

3.2.2. Reactor concentrations

In biological processes, the removal of soluble carbon is promoted mainly by microbial activity (cell reproduction) with further removal via microorganism sedimentation and the particulate carbon (e.g. in solids) is removed directly by sedimentation strategies. The microbial activity is represented by the oxygen uptake rate (OUR) (Figure 8(2)), and the most important microorganisms' biomass communities: heterotrophic-OHO, nitrifiers-AOB, denitrifying-NOB, and phosphorus-accumulating organisms (PAOs) (Figure 8(4)). With the influent overload, the carbonaceous OUR increases from 9.87 mg O/L*h of HKWW to 23.34 mg O/L*h of CWW (Figure 8(2)), demanding even more phosphorus to compensate for the peak loading, as found by Nowak *et al.* (1996). The CWW stream contains high particulate and a soluble biodegradable COD fraction (S_s and X_S) that enhance the presence of OHO microorganisms from 482 mg OHO/L of HKWW to 836 mg OHO/L of CWW (Figure 8(4)) and its posterior BOD removal (susceptible to being transformed by OHO) for cell up-taking, maintenance, and conversion into CO_2. This result suggests that the differential overload of CWW had a slight positive impact on the BOD removal. On the other hand, the high particulate inert carbon content (X_I) with poor settleability of SVI = 459 mm/h for the HKWW and SVI = 508 mm/h for the CWW impacts the overall TSS removal, in both the SBR system (Figure 8(3)) and at the effluent (Figure 9(4)).

Nitrification did not occur for HKWW nor CWW, and thus, neither for denitrification. ANO microorganisms did not grow in the SBR system for the whole simulation campaign, as seen by the absence of nitrification OUR (light blue in Figure 8(2))

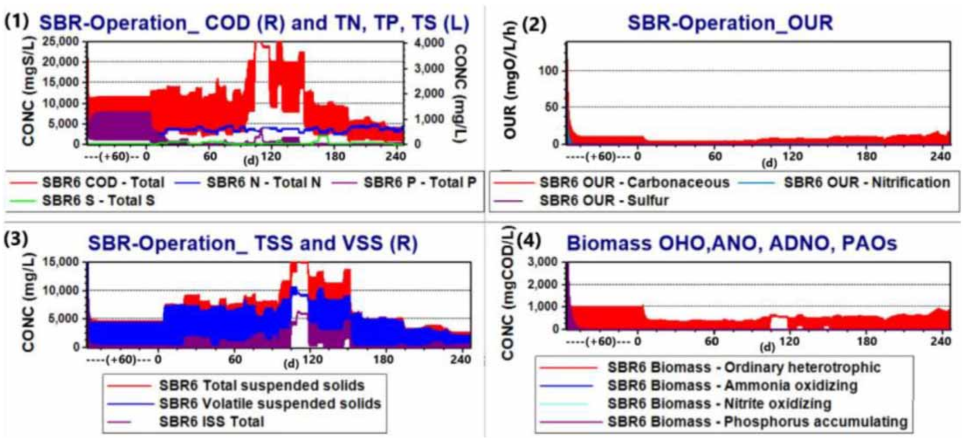

Figure 8 | SBR operation chart: for (1) nutrient concentration, (2) OUR, (3) solids as MLVSS, and (4) the most important bio-communities content.

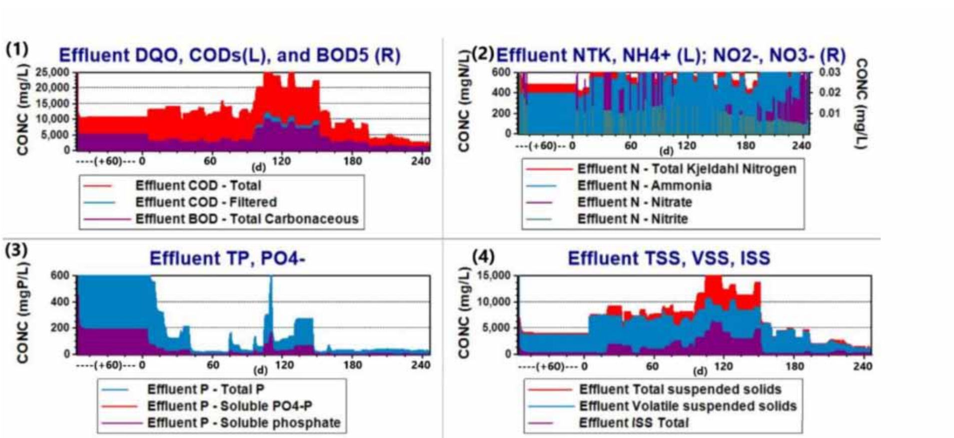

Figure 9 | Effluent performance chart: effluent concentrations for carbon (1), nitrogen (2), phosphorus (3) species, and (4) solids for the differential overload of CWW.

and ammonia-oxidizing biomass (dark blue in Figure 8(4)). This happened for multiple reasons. First, nitrifying bacteria need carbon (COD) to grow, particularly CO_2 as a carbon source. Additionally, nitrifying bacteria are sensitive to pH outside of 6.5–7.5 and reproduce slower than OHO microorganisms. Thus, if the BOD removal fails, the nitrification fails as well, because the OHO microorganisms not only produce the CO_2 that is a limiting factor but also will outcompete the nitrifying bacteria for resources (Conde & Kaparaju 2022). This fact is proven by the extent of OHO microorganisms (red line against the blue one in Figure 8(4)). Additionally, ammonia oxidizers (similar to OHO) demand phosphorus to grow, but this nutrient is in deficit. This is a result of overconsumption, due to the COD overload of HKWW in stages IV and V that demands an additional phosphorus number (Nowak *et al.* 1996) and the low or relative absence of phosphorus in the CWW (Sanghamitra *et al.* 2021).

Denitrification occurred even less than nitrification in the whole simulation study since no metabolites, such as NO_2 or NO_3, were produced from nitrification to transform in the denitrification stage. Thus, the amount of strict nitrite-oxidizing microorganisms is negligible, as is OHO, which did not denitrify properly due to the absence of enough readily biodegradable carbon sources. In prior scientific reports, authors have stated that a ratio of COD/TKN $\geq$6 would maximize nitrogen removal (Filali-Meknassi *et al.* 2004), which is specifically required for the denitrification process. However, it is important to acknowledge that most COD should be in the form of readily biodegradable carbon (S_S) fraction, especially $S_{A,}$ which is one of the main components of the CWW (Metzner & Temper 1990). Otherwise, the readily biodegradable carbon would become a limiting factor as happened to the HKWW. The aeration pattern additionally plays an important role in the growth of denitrifying microorganisms. High air inflow and even high Kla transfer increase the DO concentration or off-gases from the wastewater matrix prior to its transformation into nitrogen molecules.

3.2.3. Effluent concentration

Any stream is removing enough carbon to achieve the regulation limits from the World Bank (2007) for both soluble carbon (250 mg COD/L and 50 mg BOD/L) and particulate carbon (50 mg TSS/L). This is due to the failure of coagulation for the grease and oil removal and thus the BOD effluent concentration is still high (purpure line, Figure 9(1)). As a result, the system is prevented from removing the soluble and particulate carbon via underflow wastage (purple, Figure 5). Instead, carbon is pumped out via decant outflow (Figures 9(1) and 9(4), respectively).

As mentioned before, full nitrification/denitrification did not occur in this SBR system, and thus high NH_4^+ concentrations remained in the effluent for both wastewater matrices (blue, Figure 9(2)), and the concentrations of NO_2^- and NO_3^- as the effluent were too low (purple and green, Figure 9(2)), and did not comply with the World Bank (2007) guidelines of maximum total nitrogen (TN) of 10 mg/L. The nitrogen was not fully nitrified by autotrophs for the whole differential load project due to problems with excess aeration, pH inhibition (especially for HKWW), low alkalinity, and nutrient deficit (phosphorus, especially for CWW).

Autotroph microorganisms need non-organic carbon sources such as CO_2 and HCO_3^-, but the system faced low CO_2 production due to the low BOD removal, and this small amount of CO_2 was stripped out by the excess of aeration (as explained in Figure 11(2)). When the wastewater content has small amounts of CO_2, the low HCO_3^- tries to compensate for the CO_2 deficit by transforming itself, forced by the pH gradient (Auterská & Novák 2006), leading to an acute reduction in the alkalinity levels. In this sense, alkalinity is another source of CO_2. However, both HKWW and CWW matrices contained low alkalinity (HCO_3^-), so there was not enough non-organic carbon source for nitrifiers to thrive. Additionally, pH inhibition is another reason why nitrifiers did not grow. In both matrices, the pH was out of the optimal range for autotroph growth (6.8–7.5 pH, Figure 10). The pH inhibition reduced the growth rate of heterotroph and autotroph microorganisms by

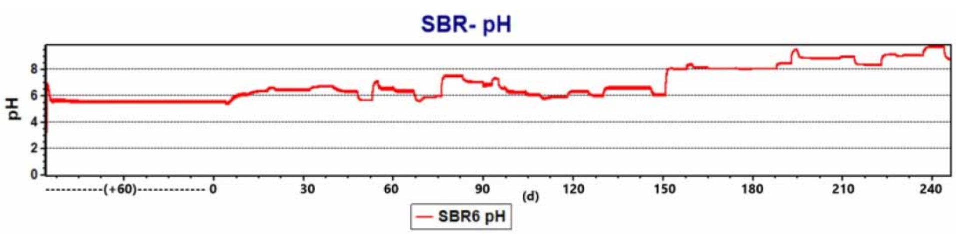

Figure 10 | pH control chart during differentia overload of CWW.

more than 50%, also related to the low alkalinity. When low alkalinity is found in wastewater, such as in HKWW, the acid (H^+) produced for ammonia oxidizers inhibits the growth of nitrate oxidizers (Chen *et al.* 2020). Additionally, the nutrient deficit is another source of nitrification inhibition, such as in the CWW stream since ANO and OHO also require phosphorus to reproduce new cells (Chen *et al.* 2020) although it seemed to be a good pH range for stages VI, VII, and VIII. Finally, for the current treatment system, the only requirement for nitrifiers that was met was the oxygen supply due to the intensive aeration.

Denitrification was not performed correctly given that the system did not nitrify and produce NO_3^- to denitrify. The high amount of oxygen did not allow the development of anoxic zones in the system and, therefore, forced the heterotrophic bacteria to take nitrate as an electroreceptor instead of oxygen. Heterotrophic microorganisms also did not have enough biodegradable carbon to produce nitrogen gas due to the low S_S content.

3.2.4. Reactor pH concentration

The pH changed from acidic in HKWW to alkaline in CWW, respectively (Figure 10). HKWW contained low alkalinity concentration and the CO_2 loss promoted the reduction in the alkalinity content, as mentioned before. On the other hand, nitrogen aided in the alkalinity found in the CWW since the ammonia, which was produced during the hydrolysis process and catalyzed by the heat process in the cooker-batch equipment, reacted with CO_2 to form ammonium bicarbonate (NH_4HCO_3), contributing to the alkalinity in the reactor (Nakhla *et al.* 2006). This created a harsh environmental condition with a pH as high as 8, hindering the biological removal and reconfirming that the low nitrogen removal was happening due to physical conditions instead of biological ones. As Brønd & Sund (1994) suggested, sufficient upstream buffering should be ensured to prevent shock loads.

3.3. Gaseous phases

Although neither oxygen, carbon dioxide, ammonia gas nor nitrous oxides were empirically recorded during the measure campaign, the gaseous phases were essential for the general pollutant change and explanation. Thus, it will be presented as the main result of the gaseous phase, based on the input provided by the simulations.

The general system presents an excess of aeration due to the high occurrence of intermittent aeration (high KLa coefficient) demonstrated by the simulations. This excessive aeration caused the loss of around 20% of the oxygen (Figure 11(1)). Additionally, the majority of the transformed carbon by OHO was taken out of the system by aeration (around 60% of CO_2, Figure 11(1)), which limited the nitrification process, particularly for the HKWW. For the CWW, CO_2 loss was less given that the gradient was inclined to form NH_4HCO_3 and increased the alkalinity, as mentioned before.

The equilibrium between ammonia gas (NH_3) and ammonium (NH_4) was heavily impacted by the pH, thus, the CWW lost most of its nitrogen in the form of NH_3 (approximately 86%), given that the basic pH favored its existence and was released by the strong aeration pattern. As presented in Figure 11(3), this nitrogen removal process was due to a physical phenomenon rather than a biological process as should have occurred. Additionally, when HKWW or CWW are discharged in natural

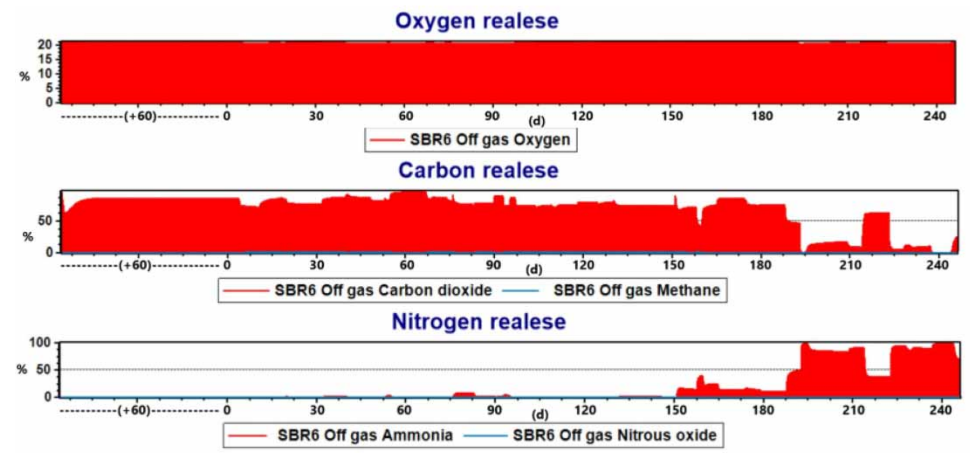

Figure 11 | Integrated off-gas phase chart % of release of (1) oxygen, (2) carbon, and (3) nitrogen species during differential overload of CWW.

water bodies under acidic and anaerobic conditions, there is an increase in the probability of releasing high nitrogen oxide emissions into the atmosphere. However, the excess of aeration in the HKWW and the basic environment of CWW did not promote the formation of this kind of greenhouse gas (GHG), as shown in Figure 11(3). These findings suggest that with proper control and monitoring, GHG emissions could be avoided without stopping the use of biological treatments (Tian *et al.* 2020).

4. CONCLUSION

The influent carbon overload (stages IV and V) in this specific case did not physically wash microorganisms out of the system but inhibited and reduced its population by half due to the harsh environmental conditions, as demonstrated by the carbonaceous OUR and OHO biomass decrease.

Even without the occurrence of the influent overload, the particulate organic removal failed, (X_I and X_S from FOG) ruining the removal of the BOD, COD, and hereafter the nitrogen removal as well since OHO outnumbered ANO. BOD removal was impacted by the acute pH inhibition from HKWW, and the low CO_2 produced by OHO was released (approximately 60%) by the aeration pattern, preventing the system from removing the biodegradable carbon in the form of biomass, but instead via decant outflow, and as a result the differential overload of CWW barely positively impacted the BOD removal.

Neither the HKWW nor CWW ANO microorganisms were found to be developing in the SBR system due to the absence of nitrification uptake rate and ammonia-oxidizing biomass from the nutrient deficit of phosphorus (for the entire project), pH inhibition caused by LCFA and VFA, and calcium and magnesium deficit (especially for CWW). Nitrification does not develop due to pH inhibition and low CO_2. The simulation showed that nitrogen removed from the system was a consequence of the high aeration system, in the form of NH_3 (approximately 86% for CWW stages), rather than the biological conversion, as expected. Thus, the differential nitrogen overload of CWW slightly positively impacted the nitrogen removal, although it did not reach the limits of the guidelines and did not under desired environmental conditions (NH_3 instead of N_2).

The system requires adjustment in the preliminary and primary treatment with the use of biosurfactants to increase the S_S from X_S fraction, which could increase the carbon bioavailability from FOG, reduce the aeration pattern to promote nitrifier growth (CO_2 retention), and add alkali species to prevent nitrifier bacteria pH inhibition. From the perspective of meat industry simulations, it is recommended to pay special attention in further analyses to organic VFAs fractions (S_A), as well as to other VFAs (propionic, butyric, and valeric), not only acetic acid, to improve the similarity between observed and simulated data. Additionally, actual respirometry tests should be run to determine the maximum growth rates of OHO and ANO, their decay rates, and hydrolysis constants.

ACKNOWLEDGEMENTS

The authors thank the GDCON and GII groups of the Universidad de Antioquia for their support in carrying out the research. Carlos Lopez-Vasquez from the IHE Delft Institute, and Markus Ahnert from the Urban and Industrial Water Management Institute at the TU Dresden, Germany for the support in the wastewater fractionation, and calibration process, respectively. The authors thank Celeste Jenisch from Portland State University for the language editing.

FUNDING

We thank the University of Antioquia for granting the research project, especially the GDCON research group for the collected and analyzed data, and the IHE Institute for granting the scholarship to fill gaps in specific knowledge of sludge simulation.

AUTHOR CONTRIBUTIONS

E. D. D. N.-B. wrote the original draft, investigated the process, conceptualized the study, developed the methodology, visualized the work, rendered support in software, data curation, and formal analysis. D. C. R.-L. supervised the work, rendered support in initial data collection, provided the resources, wrote the reviewed and edited the article. J. C. S.-M. supervised the work, provided the resources, wrote the reviewed and edited the article.

DATA AVAILABILITY STATEMENT

All relevant data are included in the paper or its Supplementary Information.

CONFLICT OF INTEREST

The authors declare there is no conflict.

REFERENCES

Auterská, P. & Novák, L. (2006) Successful solution for high nitrogen content wastewater treatment from rendering plants, *Water Science and Technology*, **54** (10), 23–30.

Bedoić, R., Špehar, A., Puljko, J., Čuček, L., Ćosić, B., Pukšec, T. & Duić, N. (2020) Opportunities and challenges: experimental and kinetic analysis of anaerobic co-digestion of food waste and rendering industry streams for biogas production, *Renewable and Sustainable Energy Reviews*, **130**, 109951.

Brennan, B., Gunes, B., Jacobs, M. R., Lawler, J. & Regan, F. (2021) Potential viable products identified from characterization of agricultural slaughterhouse rendering wastewater, *Water*, **13** (3), 352.

Brønd, S. & Sund, C. (1994) Biological removal of nitrogen in toxic industrial effluents, high in ammonia, *Water Science and Technology*, **29** (9), 231–240.

Casellas, M., Dagot, C., Pons, M. N. & Baudu, M. (2008) Influent fractionation for the use of ASM1 to optimize urban wastewater treatment: application to the removal of C and N in a SBR, *Revue des Sciences de L'eau/Journal of Water Science*, **21** (4), 451–462.

Chen, G. H., van Loosdrecht, M. C., Ekama, G. A. & Brdjanovic, D. (2020) *Biological Wastewater Treatment: Principles, Modeling and Design*. London, UK: IWA Publishing.

Conde, E. & Kaparaju, P. (2022) Effect of temporal variation in chemical composition on methane yields of rendering plant wastewater, *Energies*, **2022** (15), 7252.

Corominas Tabares, L. (2006) *Control and Optimization of an SBR for Nitrogen Removal: From Model Calibration to Plant Operation*.

Envirosim (2021) *BioWin User Manual 5.3. (Reviewed: 2023.03.09)*. Toronto, ON, Canada: Envirosim Associates Ltd. Available at: http://www.envirosim.com/downloads/BW5Manual.pdf.

Filali-Meknassi, Y., Auriol, M., Tyagi, R. D. & Surampalli, R. Y. (2004) Treatment of slaughterhouse wastewater in a sequencing batch reactor: simulation vs experimental studies, *Environmental Technology*, **25** (1), 23–38.

Hauduc, H., Neumann, M. B., Muschalla, D., Gamerith, V., Gillot, S. & Vanrolleghem, P. A. (2015) Efficiency criteria for environmental model quality assessment: A review and its application to wastewater treatment, *Environmental Modelling & Software*, **68**, 196–204.

Klaucans, E. & Sams, K. (2018) Problems with fat, oil, and grease (FOG) in food industry wastewaters and recovered FOG recycling methods using anaerobic co-digestion: a short review, *Key Engineering Materials*, **762**, 61–68.

Kosseva, M. R. (2020) Sources, characteristics, treatment, and analyses of animal-based food wastes. In: Kosseva, M. R. & Webb, C. *Food Industry Wastes*, Cambridge, MA, USA: Academic Press, pp. 67–85.

Lopez-Vazquez, C. M., Hernández García, H. A., Buitrón Méndez, G. & Cervantes Carrillo, F. J. (2017) *Tratamiento Biológico de Aguas Residuales: Principios, Modelación Y Diseño*. London, UK: IWA Publishing.

Makinia, J. & Zaborowska, E. (2020) *Mathematical Modelling and Computer Simulation of Activated Sludge Systems*. London, UK: IWA Publishing.

Melcer, H. (2004) *Methods for Wastewater Characterization in Activated Sludge Modelling*. London, UK: IWA Publishing, pp. 61–83.

Metzner, G. & Temper, U. (1990) Operation and optimization of a full-scale fixed-bed reactor for anaerobic digestion of animal rendering wastewater, *Water Science and Technology*, **22** (1–2), 373–384.

Moreno, J. J. M., Pol, A. P., Abad, A. S. & Blasco, B. C. (2013) Using the R-MAPE index as a resistant measure of forecast accuracy, *Psicothema*, **25** (4), 500–506.

Muster-Slawitsch, B., Dow, N., Desai, D., Pinches, D., Brunner, C. & Duke, M. (2021) Membrane distillation for concentration of protein-rich waste water from meat processing, *Journal of Water Process Engineering*, **44**, 102285.

Nakhla, G., Al-Sabawi, M., Bassi, A. & Liu, V. (2003) Anaerobic treatability of high oil and grease rendering wastewater, *Journal of Hazardous Materials*, **102** (2–3), 243–255.

Nakhla, G., Liu, V. & Bassi, A. (2006) Kinetic modeling of aerobic biodegradation of high oil and grease rendering wastewater, *Bioresource Technology*, **97** (1), 131–139.

Nowak, O., Svardal, K. & Kroiss, H. (1996) The impact of phosphorus deficiency on nitrification-case study of a biological pretreatment plant for rendering plant effluent, *Water Science and Technology*, **34** (1–2), 229–236.

Oles, J. & Wilderer, P. A. (1991) Computer aided design of sequencing batch reactors based on the IAWPRC activated sludge model, *Water Science and Technology*, **23** (4–6), 1087–1095.

Orhon, D., Babuna, F. G. & Karahan, O. (2009) *Industrial Wastewater Treatment by Activated Sludge*. London, UK: IWA Publishing.

Pintor, A. M., Vilar, V. J., Botelho, C. M. & Boaventura, R. A. (2016) Oil and grease removal from wastewaters: sorption treatment as an alternative to state-of-the-art technologies. A critical review, *Chemical Engineering Journal*, **297**, 229–255.

Rieger, L., Gillot, S., Langergraber, G., Ohtsuki, T., Shaw, A., Takacs, I. & Winkler, S. (2012) *Guidelines for Using Activated Sludge Models*. London, UK: IWA Publishing.

Rodríguez, D. C., Pino, N. & Peñuela, G. (2011) Monitoring the removal of nitrogen by applying a nitrification–denitrification process in a Sequencing Batch Reactor (SBR), *Bioresource Technology*, **102** (3), 2316–2321.

Sanghamitra, P., Mazumder, D. & Mukherjee, S. (2021) Treatment of wastewater containing oil and grease by biological method-a review, *Journal of Environmental Science and Health, Part A*, **56** (4), 394–412.

Sultana, N., Roddick, F. A. & Pramanik, B. K. (2024) Fat, oil and grease wastewater and dishwashers: uncovering the link to FOG deposition, *Science of The Total Environment*, **907**, 168032.

Tian, H., Xu, R., Canadell, J. G., Thompson, R. L., Winiwarter, W., Suntharalingam, P., Davidson, E. A., Ciais, P., Jackson, R. B., Janssens-Maenhout, G., Prather, M. J., Regnier, P., Pan, N., Pan, S., Peters, G. P., Shi, H., Tubiello, F. N., Zaehle, S., Zhou, F., Arneth, A., Battaglia, G., Berthet, S., Bopp, L., Bouwman, A. F., Buitenhuis, E. T., Chang, J., Chipperfield, M. P., Dangal, S. R. S., Dlugokencky, E., Elkins, J. W., Eyre, B. D., Fu, B., Hall, B., Ito, A., Joos, F., Krummel, P. B., Landolfi, A., Laruelle, G. G., Lauerwald, R., Li, W., Lienert, S., Maavara, T., MacLeod, M., Millet, D. B., Olin, S., Patra, P. K., Prinn, R. G., Raymond, P. A., Ruiz, D. J., van der Werf, G. R., Vuichard, N., Wang, J., Weiss, R. F., Wells, K. C., Wilson, C., Yang, J. & Yao, Y. (2020) A comprehensive quantification of global nitrous oxide sources and sinks, *Nature*, **586** (7828), 248–256.

Van Loosdrecht, M. C. M., Lopez-Vazquez, C. M., Meijer, S. C. F., Hooijmans, C. M. & Brdjanovic, D. (2015) Twenty-five years of ASM1: past, present and future of wastewater treatment modelling, *Journal of Hydroinformatics*, **17**, 4–5.

World Bank Group (2007). Environmental, Health and Safety (EHS) Guidelines for Meat Processing. General EHS Guidelines: Environmental Wastewater and Ambient Water Quality. [Updated: 2013-11-15]. Available at: http://www.ifc.org/ehsguidelines (Accessed: 24-November-2020).

First received 13 October 2024; accepted in revised form 21 February 2025. Available online 5 March 2025